Metamorphic evolution of high-alumina metapelites near the Panimba overthrust (Yenisei Range): Mineral associations, PT-conditions, and tectonic model

Article *in* Russian Geology and Geophysics · August 2001

CITATIONS
34

READS
121

7 authors, including:

Igor Likhanov
Sobolev Institute of Geology and Mineralogy
181 PUBLICATIONS **1,768** CITATIONS
SEE PROFILE

Oleg Petrovich Polyansky
Sobolev Institute of Geology and Mineralogy
99 PUBLICATIONS **682** CITATIONS
SEE PROFILE

Reverdatto Vladimir
Sobolev Institute of Geology and Mineralogy
238 PUBLICATIONS **2,028** CITATIONS
SEE PROFILE

P. S. Kozlov
Институт геологии и минералогии Сибирского отделения Российской ак…
58 PUBLICATIONS **780** CITATIONS
SEE PROFILE

Russian Geology and Geophysics
Vol. 42, No. 8, pp. 1138-1154, 2001

Geologiya i Geofizika
UDC 551.25

METAMORPHIC EVOLUTION OF HIGH-ALUMINA METAPELITES NEAR THE PANIMBA OVERTHRUST (*Yenisei Range*): MINERAL ASSOCIATIONS, *P-T* CONDITIONS, AND TECTONIC MODEL

I. I. Likhanov, O. P. Polyanskii, V. V. Reverdatto, P. S. Kozlov, A. E. Vershinin, M. Krebs*, and I. Memmi**

Institute of Mineralogy and Petrography, Siberian Branch of the RAS, prosp. Akad. Koptyuga 3, Novosibirsk, 630090, Russia
** Institute of Mineralogy at the University of Bochum, D-44780, Bochum, Germany*
*** Siena University, 53100, Siena, Italy*

An attempt is made to study pressure-heterogeneous high-alumina metapelites of andalusite-sillimanite and kyanite-sillimanite facies series for clearing up the *P-T* evolution of metamorphism related to thrusting tectonics. As a result of detailed research with the use of geothermobarometry and THERMOCALC-based analysis of mineral equilibria, *P-T* conditions were estimated and *P-T* paths of evolution were plotted for moderate and elevated pressures. The variability of *P-T* conditions of metamorphism suggests that the kyanite substitution for andalusite and other mineral transformations were caused by an increase in pressure under low geothermal gradient, described by a model for tectonic thickening of the crust in the zone of the Panimba overthrust. The fact that there is no marked increase in temperature on thrusting is explained by specific behavior of stationary geotherms for different kinds of rocks that have different thermophysical and heat-producing properties.
High-alumina metapelites, thermobarometry, P-T paths, tectonic model, Yenisei Range

INTRODUCTION

Of the progressive mineral reactions between polymorphous modifications of Al_2SiO_5, the commonest ones are substitutions of andalusite or kyanite by sillimanite, typical of the zonal metamorphic complexes of low and moderate pressures [1]. Within the trans-Angarian part of the Yenisei, at the headwaters of the Chapa River, andalusite substitution by kyanite was first described [2], indicating pressure growth during metamorphism. South of this region, all polymorphs of Al_2SiO_5 occur and an andalusite-kyanite isograde is mapped within a limited area in the Eruda and Chirimba basins [3]. Replacement of andalusite by kyanite at the progressive stage of metamorphism is quite rare, because the stationary continental geotherm does not usually cross the andalusite-kyanite equilibrium line [1]. Only few examples have been described in literature, with the progressive andalusite-to-kyanite transformations explained either by metastable behavior of andalusite in the *P-T* domain of kyanite stability [4] or by an increase in pressure as a result of overthrusts [5–11] or magmatic "load" (i.e., an increase in lithostatic pressure under the effect of an intrusive body) [12–14], characterized by different *P-T* paths. We have studied in detail an area in the Eruda and Chirimba basins, where regional and contact metamorphism is expressed near the tectonic fault and granite pluton. The results obtained are discussed in the context of the tectonic models available.

Given the relationships between the *P-T* evolution and tectonic history are established in a correct way, the metamorphic parageneses provide the required information on thermodynamic transformations of rocks [15]. The data on mineralogy allowed us to establish *P-T* paths of metamorphic evolution. On the basis of the calculated *P-T* paths we tried to get insight into the mechanisms responsible for the progressive andalusite-to-kyanite transformations. The tectonopetrological information was used to construct and analyze the model

of *P-T* evolution of the metamorphic complex near the Panimba thrust in the trans-Angarian part of the Yenisei Range.

GEOLOGIC SETTING

The trans-Angarian part of the Yenisei Range is the area of display of the Baikalian orogeny. Structurally, it belongs to the southwestern framing of the Siberian Platform; in the west, it borders the West Siberian Plate, and in the southeast, the Altai-Sayan folded area. Precambrian intrusive and sedimentary-metamorphic formations, ranging from Lower Proterozoic through Vendian, participate in its structure. The metamorphic rocks regionally metamorphosed under greenschist and epidote-amphibolite facies conditions amount to about 80% of the volume of the Precambrian section [16]. The most important feature of metamorphic complexes of this region is that the metamorphism is heterogeneous in pressure regime, as expressed in two facies series of regional metamorphism: andalusite-sillimanite and kyanite-sillimanite [17, 18]. The kyanite-sillimanite type of metamorphism follows the low-pressure metamorphism and is locally controlled by fault tectonics. In the area under study, the field of occurrence of metapelites of this kind is limited in the east by the Panimba thrust of northwestern strike, northeast of which Lower Proterozoic metacarbonates of the Penchenga Formation occur.

Our study was given to the low-pressure regional metamorphic rocks of andalusite-sillimanite type of the Korda Formation, widespread in the Eruda and Chirimba basins. Their Middle Riphean age is genetically related to the intracrustal origin of the granite gneisses of the Teya complex (1100± 50 Ma from U-Pb datings for zircon) [19]. Here, the low-pressure metapelites represented by the mineral assemblage muscovite+chlorite+biotite+andalusite+quartz+graphite+ilmenite ± cordierite ± chloritoid ± plagioclase (this list includes the greatest number of phases) have been metamorphosed under conditions of greenschist and epidote-amphibolite facies. Near the thrust, these rocks have experienced the moderate-pressure dislocation metamorphism of kyanite-sillimanite type of Late Riphean age (800± 50 Ma according to K-Ar dating for biotite) [20] (Fig. 1). The moderate-pressure metapelites of kyanite-sillimanite type represented by the parageneses muscovite+chlorite+biotite+quartz+kyanite+staurolite+graphite+ilmenite ± garnet ± andalusite ± chlorite ± sillimanite ± plagioclase originated under conditions of kyanite-staurolite subfacies of kyanite schist facies [21]. They make up a zone of 5 to 7 km wide and more than 20 km long, bordered by the Panimba thrust in the northeast. A specific feature of the internal structure of the zone is a change of mineral parageneses across the strike. The transition from low-pressure regional metamorphic rocks to moderate-pressure metamorphic rocks is recorded by the andalusite-kyanite isograde [3]. The predominant kinds of rock dislocations are general parallel and lenticular foliation, cleavage, boudinage, cataclasis, etc. Mylonitization is displayed locally, near the Panimba thrust.

METAMORPHIC ZONES, MINERAL ASSEMBLAGES, AND STRUCTURAL RELATIONSHIPS BETWEEN MINERALS

Carbonaceous andalusite-bearing metapelites of the Korda Formation (zone I, see Fig. 1) are widespread 5–7 km southwest of the Panimba thrust. Not subjected to kyanite-sillimanite metamorphism, they show distinct prograde metamorphic zoning [17]. They were metamorphosed under low *P-T* conditions; in appearance, they are gray and dark-gray rocks with fine-grained foliated mica-quartz-plagioclase groundmass, with large idioblasts of andalusite recognized against its background. Thin sections of the groundmass show its lepidogranoblastic texture. The following parageneses are commonest in the area under study: And+Ms+Bt+Chl+Qtz, And+Ms+Bt+Qtz+Crd, And+Ms+Bt+Qtz+Chl+Pl, and And+Ms+Bt+Chl+Cld+Qtz. The mineral symbols are borrowed from [22]. The andalusite crystals are plane-parallel to lamination, are of pink color, have a distinct idioblastic habit, and measure up to 2 cm across and 8 cm along. The rock may contain up to 10–15 vol.% andalusite. Graphite inclusions in andalusite impart it either hourglass or chiastolite-cross texture, visible in thin sections. Inclusions in the groundmass and chiastolite are oriented equally. Quartz forms isometric elongate or irregular grains with smooth or serrated outline, 0.1 to 2 mm in size. Muscovite occurs either as solitary flakes 0.05 to 1.5 mm long or as aggregates between quartz grains. Plagioclase exists in the form of irregular grains up to 0.5 mm across or elongated in plane of foliation. Biotite and chlorite occur in the form of irregular flakes measuring up to 2 mm across. The ore mineral is ilmenite, which forms plates lying in the plane of foliation and irregular grains. Occasionally, the rocks contain chloritoid and, less frequently, cordierite. Idiomorphic prismatic and tabular crystals of chloritoid up to 1 mm in size are parallel

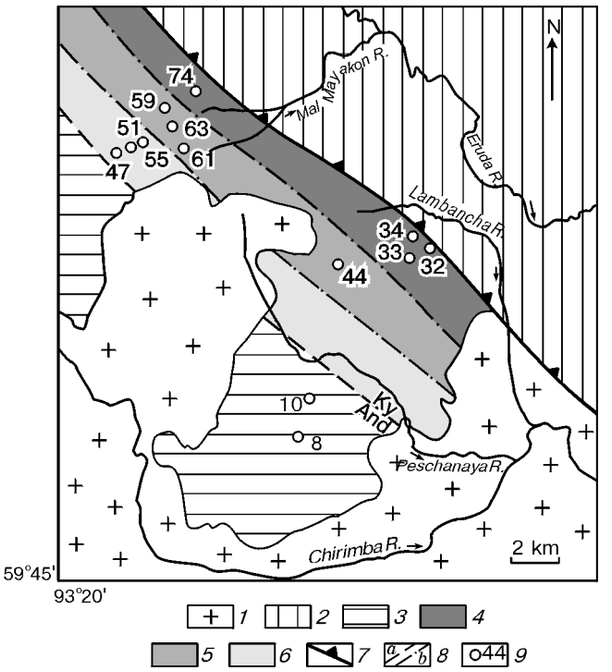

Fig. 1. A schematic map of metamorphism in the Eruda-Chirimba interfluve, trans-Angarian part of the Yenisei Ridge (based on the materials obtained by the Tsentralnaya team of the Angara Geological Prospecting Expedition, including data of a detailed (1:50,000) geological survey and additional geological exploration of areas in the southern part of the North-Yenisei region (authors are Yu. F. Avdievskii, A. I. Vyzu, and P. S. Kozlov) [17]. ***1*** **— granites of the Chirimba Massif;** ***2*** **— metaaleurolites and metacarbonates of the Penchenga Formation;** ***3*** **— Korda metapelites of the And-Sil facies series (I); Korda metapelites of Ky-Sil type;** ***4*** **— inner zone (IV),** ***5*** **— intermediate zone (III),** ***6*** **— outer zone (II);** ***7*** **— Panimba thrust;** ***8*** **— And-Ky isograde (*a*) and boundaries between zones of the Ky-Sil-type metapelites of the Korda Formation (*b*);** ***9*** **— sampling localities.**

to foliation. Cordierite is usually found in the form of inclusion-oversaturated ellipsoid poikiloblasts 0.5 to 8 mm in diameter, accompanied by randomly oriented flakes of biotite and muscovite. Graphite is common in the groundmass, existing in the form of small particles up to 0.1 mm across and dust-like accumulations. Accessory minerals are tourmaline, margarite, and calcite.

Closer to the Panimba thrust, three zones are recognized according to characteristics of texture and composition of metamorphosed metapelites: outer (II), intermediate (III), and internal (IV) (see Fig. 1). Mineral composition of all these zones is nearly the same. Moderate-pressure metapelites of kyanite-sillimanite type within these zones are represented by the following parageneses: Ms+Bt+Qtz+Grt+St+Ky+Pl (the most frequent), Ms+Bt+Qtz+Grt+St+Ky, Ms+Bt+Qtz+Grt+St+Ky+Cld, Ms+Bt+Qtz+Grt+St+Chl, Ms+Bt+Qtz+Ky+Grt+Sil, Ms+Bt+Qtz+Grt+St+Ky+Sil+And (relict). The small-aggregate groundmass (with grains measuring 0.005 to 0.01 mm) never contains kyanite, which indicates that it appeared under specific conditions. Near the Panimba thrust, the content of relict andalusite in the rocks decreases, while amounts of kyanite, staurolite, and garnet increase. Zone II is characterized by manifestation of obvious cataclasis of crystals of andalusite, locally replaced by a kyanite-muscovite-staurolite aggregate in cracks, on periphery, and along the diagonal of “chiastolite cross”. Relict decomposed andalusite remains in the central parts of pseudomorphs. The development of pseudomorphs is visualized as the porphyroblasts of andalusite become gray and irregular because of differently oriented prisms and radial sheaf-like aggregates of the newly formed kyanite. The outer prismatic form of andalusite crystals in this case remains the same. The substitution of andalusite by a complex of minerals implies that a complicated polymorphous transition took place. A possible mechanism for the observed substitution is cation exchange [23, 24]. Staurolite forms two types of grains: large well-cut porphyroblasts (up to 1.5 cm) and small (0.05–0.2 mm) crystals. Large grains of staurolite

usually contain aggregates of vermicular inclusions of quartz, creating a pattern on the surface, as well as small relict inclusions of andalusite, chlorite, chloritoid, and muscovite, entrapped during its growth. Muscovite inside the pseudomorphs occurs as randomly oriented flakes unlike the groundmass where it is aligned parallel to the secondary foliation. In places, it occurs in mutual intergrowths with margarite to form fine- and medium-grained aggregates. The garnet grains growing in mica-enriched interbeds have an idiomorphous habit, unlike the skeletal and irregular forms from the sites made up chiefly of quartz. The most resorbed grains of garnet occur near or in monomineral quartz veins and lenses. Inclusions in garnet are ilmenite, muscovite, biotite, and quartz. The biotite have kink bands, with disturbed edges turned toward the secondary foliation.

Intermediate zone III is represented by products of metapelite deformation. Here, andalusite, partly or completely substituted by kyanite-muscovite-staurolite pseudomorphs, is recrystallized to a higher degree than it is in zone II. The square cross sections of sheared andalusite-kyanite pseudomorphs are shaped like lozenges, with the interstices between them filled with pressure-shadow structures of recrystallized quartz. The three polymorphous modifications of Al_2SiO_5 (andalusite, kyanite, and sillimanite) coexist only within this zone (sp. 44 and 61) near the granitoid intrusion. Sillimanite is usually represented by fibrolite and rarely has a prismatic habit, developed on the edges of kyanite grains or in andalusite crystals along cleavage. Though the three aluminosilicate polymorphs are actually present in the rock, there is no evidence that they were in equilibrium with one another. Unlike andalusite, which is the earliest phase, two other modifications, kyanite and sillimanite, cannot be arranged in time for sure. Still closer to the Panimba thrust, the last relics of andalusite dissapear, which spatially coincides with the transition to the inner zone. In blastoclasites, large and, partly, small grains of garnet are fragmented and dissipated over steep microcleavage planes. The small-aggregate mineral mass making up the rock matrix is distinctly oriented over the plane of cleavage and secondary foliation to flow gently around relics of andalusite and its pseudomorphs and broken grains of garnet, often with tongues reaching intra- and intergranular spaces. The secondary foliation was, first of all, expressed in a gradual decrease in grain size. Inner zone IV, adjacent to the Panimba thrust from the southwest, is distinguished by the complete recrystallization of mineral matter with the formation of blastomylonites. Lozenge-like aggregates (pseudomorphs after andalusite), filled with aggregated kyanite, staurolite, and muscovite, transform into lenses, whose long axis is aligned parallel to the foliation. Unlike well-cut rhombododecahedra of preliminary zones from mica-enriched sites of the rock, garnet in the inner zone has the shape of flattened discoid porphyroblasts, indicating that the crystals grew under stress. Additional evidence comes from the presence of lenticular-nodular structure resulting from the tectonic reworking of pseudomorphs after andalusite, veins and lenses of granulated quartz occurring in a band of deformation concordant with the strike of thrust. In places, individual grains of garnet underwent rotation to form snow-ball structures. Numerous signatures of boudinage and plastic flow with developed lenticular and drop-like mineral segregations are also observed there.

ANALYTICAL METHODS. CHEMICAL COMPOSITIONS OF ROCKS AND MINERALS

The bulk chemical composition of rocks has been established using a multichannel X-ray fluorescent spectrometer CPM-25 at the United Institute of Geology, Geophysics and Mineralogy, Novosibirsk. The data obtained over 13 chemical analyses of samples of metapelites from different zones (Table 1) show variations in rock composition, with 57.14 to 62.59 wt.% SiO_2, 6.36 to 12.87 wt.% Fe_2O_3, and 0.26 to 1.06 wt.% CaO. Differences in contents of these components may be related to heterogeneities of rocks enriched in quartz and micas to a different degree and to changes in amounts of plagioclase and calcite. As compared with average compositions of ordinary metapelites [25], the explored rocks are enriched in K_2O and depleted in CaO and Na_2O. In general, however, these rocks are classified as metapelites enriched in Fe (X_{Fe} = FeO/(FeO+MgO+MnO) = 0.6–0.76 on mole base) and in Al (X_{Al} = Al_2O_3–$3K_2O$/(Al_2O_3–$3K_2O$+FeO+MgO+MnO) = 0.30–0.48) [26, 27]. On the triangluar AFM diagram [28], the chemical compositions of all rocks lie above the garnet–chlorite tie line (Fig. 2).

Thirteen thin sections of diagnostical rocks from different zones were prepared for microprobe analyses. Their locations are numbered in Fig. 1. The chemical composition of mineral phases in metapelites has been established by means of an EDAX DX-4 X-ray energy-dispersion microprobe, connected with a Philips XL-30 microscope, at Siena University, Italy, and by means of Camebax-Micro probe at the UIGGM, Novosibirsk, and Cameca SX-50 microprobe at University of Bochum, Germany. Results are given in Table 2. Except for specimens 34, 74, 44, and 61, analyses of the cores of garnet grains are not reported here, because they were not used for determination of temperature and pressure with the help of a geothermobarometer. The presence of graphite and virtually pure ilmenite in each rock means that the oxidation potential was low and the content

Table 1

Chemical Composition of Metapelites of the Korda Formation

Component	I		II			III				IV			
	(8)	(10)	(47)	(51)	(55)	(44)	(59)	(61)	(63)	(32)	(33)	(34)	(74)
SiO_2	58.32	62.59	60.22	58.40	57.25	57.81	59.71	61.09	57.17	58.14	60.98	58.59	57.14
TiO_2	0.86	0.95	0.94	1.15	1.06	0.81	0.96	0.92	0.95	0.96	0.95	0.58	0.86
Al_2O_3	21.47	18.28	19.06	22.89	21.30	19.33	20.43	19.17	24.69	23.06	19.60	21.68	22.66
Fe_2O_3	8.29	8.64	10.30	6.36	9.15	12.87	7.48	7.41	7.96	9.80	8.19	9.01	9.63
MnO	0.07	0.07	0.11	0.17	0.25	0.12	0.03	0.05	0.05	0.11	0.09	0.15	0.04
MgO	1.54	2.81	1.92	1.19	1.53	2.36	1.89	1.89	2.03	1.99	1.99	2.81	1.52
CaO	0.23	0.20	0.24	0.97	0.34	0.42	0.27	0.20	0.31	0.25	0.26	1.06	0.31
Na_2O	0.3	0.29	0.31	0.92	1.13	0.32	0.48	0.48	0.48	0.72	0.72	0.3	0.29
K_2O	3.24	2.91	3.08	3.38	3.29	3.03	3.01	3.52	2.52	3.44	3.97	2.12	2.67
LOI	5.29	2.61	3.79	3.86	4.58	2.69	4.83	4.81	2.94	1.90	2.54	2.73	4.87
Total	99.61	99.35	99.97	99.29	99.88	99.76	99.09	99.54	99.10	100.3	99.29	99.03	99.99

Note. Analytical results are given in wt.%; total iron, Fe_2O_3. LOI, loss on ignition. I—IV, zones; parenthesized digits, number of specimen.

of Fe^{3+} in structural formulas of Fe-bearing phases is very low [29]. Accordingly, mineral stoichiomtery was calculated (see Table 2). Given below are the main regularities of variation of chemical compositions of rock-forming minerals.

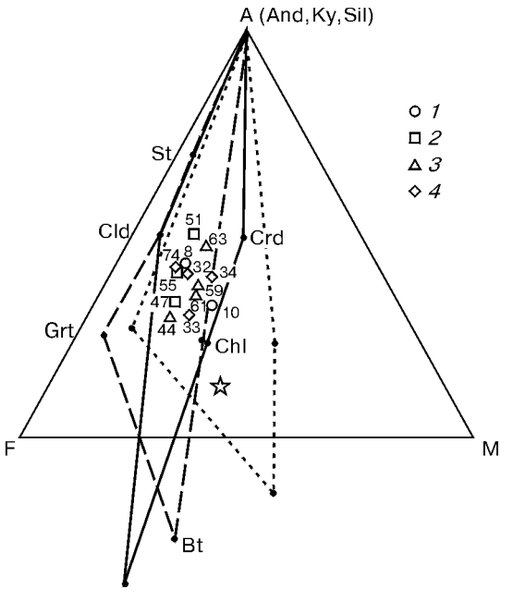

Fig. 2. AFM-diagram representing chemical compositions of rocks, minerals, and the most typical mineral assemblages. Metapelites of: *1* — And-Sil type (I), *2* — Ky-Sil type from outer zone (II), *3* — intermediate zone (III), *4* — inner zone (IV). Star indicates the average composition of typical metapelites after [26, 27]. Mineral compositions from the analyzed assemblages are shown by heavy dots. Solid lines connect minerals from metapelites of zone I, dashed lines connect those from zones II and III, and dotted lines, from zone IV. Numbers of rock and mineral compositions follow Fig. 1.

Table 2

Chemical Composition and Structural Formulas of Minerals

Component	Grt														
	II			III						IV					
	(55)r	(47)r	(51)r	(59)r	(63)r	(44)c	(44)r	(61)c	(61)r	(32)r	(33)r	(34)c	(34)r	(74)c	(74)r
SiO_2	36.78	36.82	36.74	36.25	36.41	36.29	36.22	36.14	36.26	37.40	36.83	36.88	37.40	36.05	36.11
TiO_2	0.10	0.09	0.08	0.08	0.09	0.03	0.04	0.02	0.04	0.00	0.04	0.00	0.00	0.03	0.04
Al_2O_3	20.14	20.18	20.08	20.43	20.37	20.32	20.26	20.30	20.23	21.01	20.04	20.79	20.96	20.21	20.12
FeO	38.37	38.24	38.38	38.41	38.27	38.15	38.14	37.97	38.25	33.48	38.23	33.67	33.62	38.21	38.34
MnO	2.11	2.13	2.27	2.14	2.21	2.88	2.31	2.88	2.16	0.64	2.40	0.95	0.66	3.17	2.16
MgO	1.96	1.93	1.92	1.97	1.96	2.13	2.21	2.05	2.13	3.08	1.91	3.77	3.54	2.04	1.98
CaO	0.88	0.85	0.90	1.11	1.14	0.68	1.03	0.79	1.14	4.12	1.53	2.02	3.81	0.80	1.55
Σ	100.3	100.2	100.4	100.4	100.5	100.4	100.2	100.2	100.2	99.73	100.9	99.08	99.99	100.3	100.3
	12(O)														
Si	3.00	3.01	3.00	2.96	2.97	2.96	2.96	2.96	2.97	2.99	2.99	3.01	2.99	2.96	2.96
Ti	0.01	0.01	0.01	0.01	0.01	0.00	0.00	0.00	0.00	0.00	0.00	0.00	0.00	0.00	0.00
Al	1.94	1.94	1.93	1.97	1.96	1.96	1.95	1.96	1.95	1.99	1.92	2.00	1.98	1.95	1.95
Fe	2.62	2.61	2.62	2.63	2.61	2.61	2.61	2.60	2.62	2.25	2.60	2.30	2.25	2.62	2.63
Mn	0.15	0.15	0.16	0.15	0.15	0.20	0.16	0.20	0.15	0.06	0.17	0.07	0.04	0.22	0.15
Mg	0.24	0.23	0.23	0.24	0.24	0.26	0.27	0.25	0.26	0.38	0.23	0.46	0.42	0.25	0.24
Ca	0.08	0.07	0.08	0.10	0.10	0.06	0.09	0.07	0.10	0.34	0.13	0.18	0.33	0.07	0.14
X_{Alm}	0.850	0.851	0.848	0.844	0.842	0.834	0.835	0.834	0.839	0.743	0.831	0.766	0.740	0.830	0.833
X_{Sps}	0.047	0.048	0.051	0.048	0.049	0.062	0.051	0.063	0.047	0.019	0.052	0.022	0.013	0.069	0.047
X_{Prp}	0.077	0.077	0.076	0.077	0.077	0.083	0.084	0.081	0.083	0.126	0.074	0.153	0.138	0.079	0.077
X_{Grs}	0.026	0.024	0.025	0.031	0.032	0.021	0.030	0.022	0.031	0.113	0.042	0.059	0.109	0.022	0.043

Component	Pl													
	I		II			III				IV				
	(8)r	(10)r	(55)r	(47)r	(51)r	(59)r	(63)r	(44)r	(61)r	(32)r	(33)r	(34)c	(34)r	(74)r
SiO_2	65.76	65.67	64.81	64.91	64.72	64.53	64.98	65.01	64.88	57.64	65.05	56.80	59.67	64.91
Al_2O_3	21.45	21.57	22.18	22.23	22.18	22.68	22.08	21.99	21.92	25.81	22.24	26.51	24.81	22.12
FeO	0.20	0.14	0.00	0.05	0.06	0.14	0.11	0.00	0.05	0.08	0.00	0.03	0.11	0.12
CaO	1.28	1.99	2.40	2.43	2.41	2.29	2.40	2.44	2.41	8.36	2.45	9.15	7.25	2.41
Na_2O	10.47	10.23	9.61	9.57	9.63	9.42	9.38	9.61	9.50	7.24	9.53	6.84	7.96	9.62
K_2O	0.07	0.06	0.29	0.30	0.25	0.24	0.18	0.27	0.24	0.06	0.34	0.10	0.05	0.15
Σ	99.23	99.66	99.29	99.49	99.25	99.30	99.13	99.32	99.00	99.19	99.61	99.43	99.85	99.33
	8(O)													
Si	2.90	2.89	2.87	2.86	2.86	2.85	2.87	2.87	2.87	2.61	2.87	2.57	2.67	2.87
Al	1.12	1.12	1.16	1.16	1.16	1.18	1.15	1.15	1.14	1.38	1.16	1.41	1.31	1.15
Fe	0.01	0.01	0.00	0.00	0.00	0.01	0.00	0.00	0.00	0.00	0.00	0.00	0.00	0.00
Ca	0.06	0.09	0.11	0.12	0.11	0.11	0.11	0.12	0.11	0.405	0.12	0.44	0.35	0.11
Na	0.90	0.87	0.82	0.82	0.83	0.81	0.80	0.82	0.82	0.634	0.81	0.60	0.69	0.82
K	0.00	0.00	0.02	0.02	0.01	0.01	0.01	0.02	0.01	0.00	0.02	0.01	0.00	0.00
X_{An}	0.063	0.094	0.119	0.121	0.119	0.116	0.124	0.121	0.122	0.389	0.122	0.420	0.334	0.121

Table 2 **(continued)**

Component	Bt												
	I		II			III				IV			
	(8)	(10)	(55)	(47)	(51)	(59)	(63)	(44)	(61)	(32)	(33)	(34)	(74)
SiO_2	34.92	34.52	34.80	34.82	34.62	34.75	34.61	34.74	34.46	36.94	34.70	37.14	34.75
TiO_2	1.84	1.99	3.00	2.91	2.87	3.05	2.76	2.62	2.69	1.62	3.10	1.38	2.76
Al_2O_3	18.87	19.22	19.06	19.11	19.17	19.15	19.09	19.05	19.40	19.41	18.87	19.32	19.22
FeO	23.91	24.98	22.22	22.36	22.41	22.14	22.43	22.35	21.97	17.28	22.28	16.92	22.43
MnO	0.09	0.16	0.08	0.10	0.08	0.10	0.13	0.04	0.09	0.09	0.10	0.08	0.07
MgO	6.01	6.15	7.24	7.48	7.34	7.33	7.37	7.65	7.37	11.82	7.45	12.08	7.39
Na_2O	0.18	0.14	0.19	0.16	0.15	0.20	0.18	0.19	0.18	0.28	0.14	0.53	0.17
K_2O	9.84	8.16	8.69	9.02	8.99	8.99	8.84	8.73	9.08	8.14	9.03	7.98	8.91
Σ	95.66	95.32	95.28	95.96	95.63	95.71	95.41	95.37	95.24	95.58	95.67	95.43	95.70
	11(O)												
Si	2.96	2.93	2.68	2.67	2.66	2.67	2.67	2.67	2.66	2.74	2.67	2.75	2.67
Ti	0.12	0.13	0.17	0.17	0.17	0.18	0.16	0.15	0.16	0.09	0.18	0.08	0.16
Al^{IV}	1.04	1.07	1.32	1.33	1.34	1.33	1.33	1.33	1.34	1.26	1.33	1.25	1.33
Al^{VI}	0.85	0.85	0.41	0.40	0.40	0.40	0.40	0.40	0.42	0.44	0.38	0.44	0.41
Fe	1.70	1.77	1.43	1.43	1.44	1.42	1.45	1.44	1.42	1.07	1.43	1.05	1.44
Mn	0.01	0.01	0.01	0.01	0.01	0.01	0.01	0.00	0.01	0.01	0.01	0.01	0.01
Mg	0.76	0.78	0.83	0.85	0.84	0.84	0.85	0.88	0.85	1.31	0.85	1.33	0.85
Na	0.03	0.02	0.03	0.02	0.02	0.03	0.03	0.03	0.03	0.04	0.02	0.08	0.03
K	1.07	0.88	0.85	0.88	0.88	0.88	0.87	0.86	0.89	0.77	0.89	0.75	0.87
X_{Fe}	0.691	0.694	0.633	0.601	0.632	0.628	0.630	0.621	0.626	0.450	0.627	0.441	0.629

Component	Ms												
	I		II			III				IV			
	(8)	(10)	(55)	(47)	(51)	(59)	(63)	(44)	(61)	(32)	(33)	(34)	(74)
SiO_2	45.91	47.67	45.42	46.38	46.46	45.94	46.00	45.32	45.30	47.17	44.97	47.37	45.38
TiO_2	0.55	0.23	0.62	0.25	0.26	0.54	0.51	0.65	0.52	0.29	0.54	0.48	0.60
Al_2O_3	35.98	35.83	35.85	36.75	36.56	35.96	36.36	36.21	35.28	35.86	35.37	35.33	36.51
FeO	1.03	0.72	1.35	0.93	1.04	1.06	1.27	1.49	1.75	0.66	1.78	0.87	1.23
MgO	0.58	0.39	0.58	0.39	0.48	0.63	0.59	0.53	0.68	0.82	0.61	1.20	0.51
Na_2O	0.71	0.55	0.73	1.96	1.37	0.72	0.78	0.60	0.68	0.70	0.74	1.03	0.91
K_2O	10.46	8.94	10.11	8.64	9.20	10.24	10.33	10.58	10.08	9.46	10.09	8.66	10.05
Σ	95.22	94.35	94.66	95.30	94.37	95.09	95.84	95.38	94.29	94.96	94.10	94.94	95.19
	11(O)												
Si	3.05	3.15	3.04	3.06	3.07	3.06	3.04	3.02	3.04	3.11	3.04	3.12	3.02
Ti	0.03	0.01	0.03	0.01	0.01	0.03	0.03	0.03	0.03	0.02	0.03	0.03	0.03
Al^{IV}	0.95	0.85	0.96	0.94	0.93	0.94	0.96	0.98	0.96	0.89	0.96	0.88	0.98
Al^{VI}	1.87	1.94	1.87	1.91	1.91	1.88	1.87	1.86	1.87	1.90	1.86	1.87	1.88
Fe	0.06	0.04	0.08	0.05	0.06	0.06	0.07	0.08	0.08	0.04	0.10	0.05	0.07
Mg	0.06	0.04	0.06	0.04	0.05	0.06	0.06	0.05	0.06	0.08	0.06	0.12	0.05
Na	0.09	0.07	0.10	0.25	0.18	0.09	0.10	0.08	0.10	0.09	0.10	0.13	0.12
K	0.89	0.75	0.86	0.73	0.77	0.87	0.87	0.90	0.86	0.80	0.87	0.73	0.85
X_{Na}	0.092	0.085	0.104	0.255	0.189	0.094	0.103	0.082	0.104	0.101	0.103	0.151	0.123

Table 2 **(continued)**

Component	Chl			Cld			St		Ilm	And	Ky	Sil	Crd	Mrg	Tur
	I		II	IV	I	III	II	IV	II	III	IV	III	I	I	IV
	(8)	(10)	(55)	(74)	(8)	(63)	(55)	(74)	(51)	(63)	(33)	(44)	(10)	(10)	(33)
SiO_2	23.01	24.37	22.79	23.34	24.14	23.88	26.99	27.37	0.03	36.36	36.42	36.33	48.32	30.01	36.87
TiO_2	0.14	0.04	0.24	0.16	0.00	0.01	0.04	0.08	53.79	0.00	0.02	0.05	0.04	0.04	0.69
Al_2O_3	21.72	22.52	21.72	22.63	40.48	40.67	54.26	54.43	0.03	63.52	63.38	63.12	30.86	50.61	34.16
FeO	30.00	29.92	30.54	31.09	25.33	24.97	14.48	14.64	44.40	0.23	0.22	0.37	11.27	0.42	9.19
MnO	0.12	0.10	0.08	0.06	0.28	0.29	0.16	0.11	0.79	0.02	0.00	0.01	0.19	0.04	0.01
MgO	10.85	10.75	10.54	10.62	2.13	1.98	1.17	1.19	0.04	0.00	0.04	0.08	6.18	0.13	4.47
CaO	0.00	0.00	0.02	0.00	0.00	0.01	0.00	0.03	0.00	0.00	0.00	0.02	0.03	12.37	0.19
Na_2O	0.11	0.00	0.12	0.04	0.05	0.00	0.00	0.00	0.00	0.02	0.02	0.03	0.77	0.93	1.56
K_2O	0.05	0.00	0.03	0.03	0.00	0.03	0.00	0.01	0.00	0.02	0.00	0.03	0.00	0.02	0.08
ZnO	0.00	0.00	0.00	0.00	0.06	0.09	0.99	0.92	0.00	0.00	0.00	0.03	0.00	0.00	0.08
Σ	86.00	87.70	86.08	87.97	92.47	91.93	98.09	98.78	99.08	100.2	100.1	100.1	97.66	94.57	87.30
		14(O)			12(O)		48(O)		3(O)		5(O)		18(O)	11(O)	31(O)
Si	2.55	2.63	2.53	2.54	2.01	1.99	7.87	7.92	0.00	0.98	0.98	0.98	5.09	2.01	6.21
Ti	0.01	0.00	0.02	0.01	0.00	0.00	0.01	0.02	1.02	0.00	0.00	0.00	0.00	0.00	0.09
Al	2.84	2.87	2.86	2.90	3.96	4.00	18.63	18.56	0.00	2.02	2.02	2.01	3.83	3.99	6.78
Fe	2.78	2.70	2.84	2.82	1.76	1.74	3.53	3.54	0.94	0.01	0.01	0.01	0.99	0.02	1.29
Mn	0.01	0.01	0.01	0.01	0.02	0.02	0.04	0.03	0.02	0.00	0.00	0.00	0.02	0.00	0.00
Mg	1.79	1.73	1.75	1.72	0.26	0.25	0.51	0.51	0.00	0.00	0.00	0.00	0.97	0.01	1.12
Ca	0.00	0.00	0.00	0.00	0.00	0.00	0.00	0.01	0.00	0.00	0.00	0.00	0.00	0.89	0.03
Na	0.02	0.00	0.03	0.01	0.01	0.00	0.00	0.00	0.00	0.00	0.00	0.00	0.16	0.12	0.51
K	0.01	0.00	0.00	0.00	0.00	0.00	0.00	0.00	0.00	0.00	0.00	0.00	0.00	0.00	0.01
Zn	0.00	0.00	0.00	0.00	0.00	0.01	0.21	0.20	0.00	0.00	0.00	0.00	0.00	0.00	0.01
X_{Fe}	0.608	0.609	0.619	0.621	0.871	0.874	0.874	0.874	—	—	—	—	0.505	—	0.535

Note. X_{Alm} = Fe/(Fe+Mg+Mn+Ca), X_{Prp} = Mg/(Fe+Mg+Mn+Ca), X_{Sps} = Mn/(Fe+Mg+Mn+Ca), X_{Grs} = Ca/(Fe+Mg+Mn+Ca), X_{Fe} = Fe/(Fe+Mg), X_{Na} = Na/(Na+K), X_{An} = Ca/(Ca+Na+K). Total iron is given in the form of FeO; 0.00, beyond the microprobe sensitivity; Σ, total in wt.%. Structural formulas of minerals are calculated for a fixed number of oxygen atoms designated as *n*(O); c, core; r, rim.

The chemical composition of *andalusite, kyanite, and sillimanite* is close to pure Al_2SiO_5 (within the microprobe sensitivity) with traces of Fe (<0.01 atoms per a formula unit).

In composition, the majority of *garnets* from different zones are similar to each other, varying in a narrow range, $Alm_{83–85}$, $Prp_{7–8}$, $Sps_{4–7}$, $Grs_{2–4}$, with an insignificant change in Fe content, X_{Fe} = 0.91–0.92. The prograde zoning of garnets is dictated by a gradual increase in grossular and decrease in spessartine components from core to rim of grains with virtually constant contents of almandine and pyrope components (see Table 2, Fig. 3). An exception is garnets in association with magnesian biotite and chlorite and zonal andesine from Mg-richer rocks of inner zone IV, characterized by a considerable increase in grossular component and weak decrease in spessartine, almandine, and pyrope components with an insignificant change in Fe content, X_{Fe} = 0.83–0.84 (see Table 2, Fig. 3).

Chemical composition of *staurolite* is nearly the same in all the specimens examined. Typically, they have

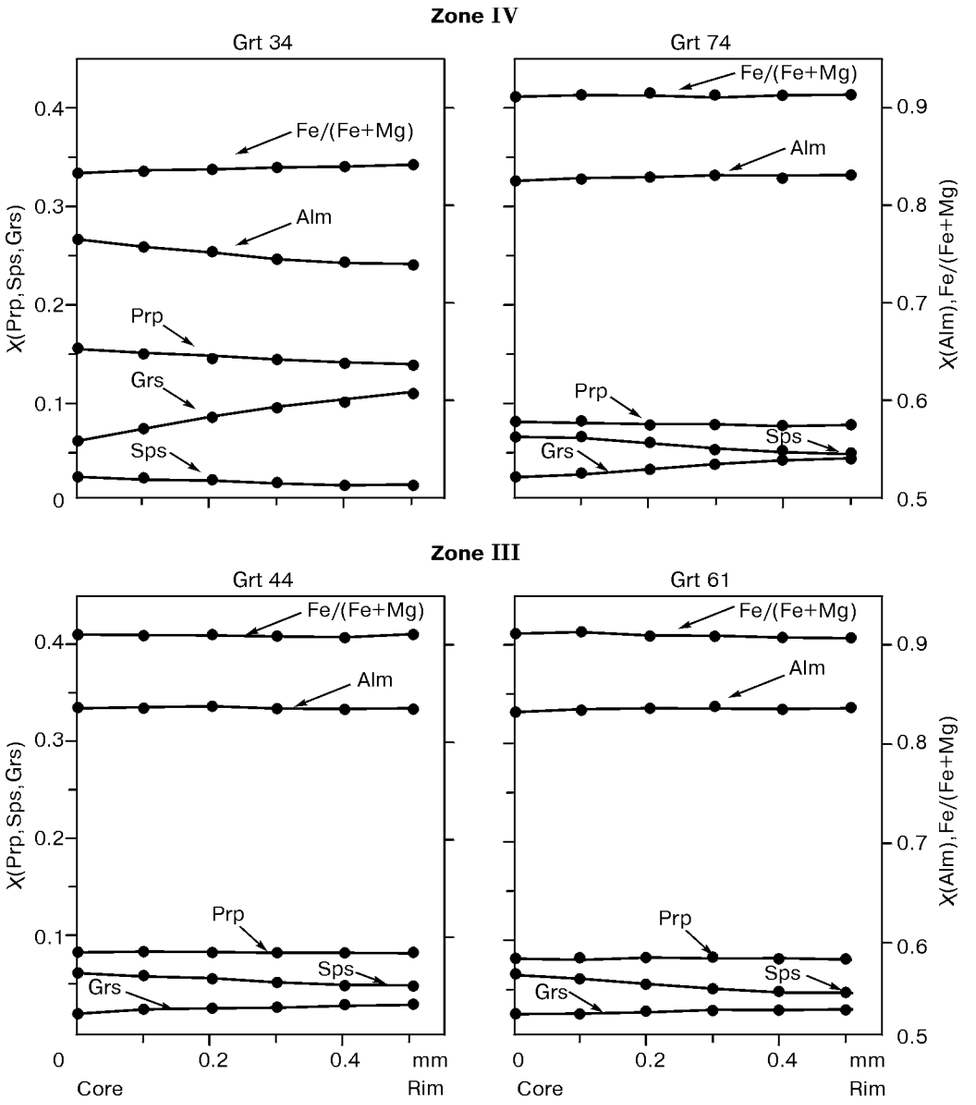

Fig. 3. Concentration profiles for garnets from species of intermediate zone III and inner zone IV.

low and slightly variable contents of MnO (0.11–0.16 wt.%) and ZnO (0.92–0.99 wt.%). The mineral shows no zoning, X_{Fe} = 0.874, i.e., lower than in the majority of coexisting garnets.

Biotite shows no zoning, and the chemical composition of its grains at the contact with and far from garnet is the same. In the transition from zone I to zones II–IV, tbe content of Al^{IV} in the mineral increases from 1.04–1.07 to 1.25–1.34 with XFe decreased from 0.69 to 0.603. The Mg-richest biotites from parageneses with Mg-rich chlorite and garnet (X_{Fe} = 0.441–0.450) occur in inner zone IV (sp. 32, 34).

Muscovite is characterized by slight variations in contents of celadonite component (Mg+Fe)/(Mg+Fe+Al ^{VI}) from 0.08 to 0.16, and considerable changes in paragonite component (X_{Na}) from 0.085 to 0.255. Compositions of muscovite grains inside pseudomorphs after andalusite and in the groundmass are identical.

Plagioclase is usually homogeneous. Its composition varies from albite X_{An} = 0.063–0.094 in zone I to oligoclase X_{An} = 0.116–0.124 in zones II–IV. A drastic jump in the content of anorthite component to andesine occurs in an inner zone (sp. 32 and 34), where the mineral shows normal zoning with the anorthite-enriched core (X_{An} = 0.42) as compared with the rim (X_{An} = 0.334).

Chlorite is chemically uniform in all specimens with small variations of iron content (X_{Fe} = 0.608–0.621), except for sp. 34 with X_{Fe} = 0.410.

Chloritoid has no zoning, with constant X_{Fe} = 0.871–0.874.

Composition of *ilmenite* is close to the stoichiometric formula with a constant content of Mn (0.02).

Composition of *margarite* is close to the ideal formula, usually $Mrg_{88}Pg_{12}$.

Tourmaline is aluminous schorl-dravite with X_{Fe} = 0.535.

All the specimens contain a small amount of *calcite* with FeO reaching 2.76 wt.%.

Cordierite is chemically uniform, with 0.77 wt.% Na_2O and X_{Fe} = 0.505.

THERMODYNAMIC CONDITIONS OF METAMORPHISM OF METAPELITES

In petrological studies of metamorphic rocks, two approaches of quantitative thermobarometry are commonly used to clear up a geodynamic setting. The first approach is the traditional "absolute" geothermometry, oriented chiefly toward the determination of maximum pressures and peak temperatures for the minerals existing in approximate chemical equilibrium. The second approach, "relative" thermobarometry, includes the determination of depths and thermal structure provided that the mineral phases of metamorphic rocks are close to equilibrium. The end result of "relative" thermobarometry is *P-T* paths, on the basis of which the evolution of metamorphic rocks in time can be constructed. Though, compared with the peak conditions of metamorphism, the *P-T* paths of evolution yield more information for the estimation of mechanisms of geodynamic processes, both approaches must be used to obtain a complete description of a metamorphic rock [30].

Geothermobarometry. For metamorphic rocks of andalusite-sillimanite type temperatures were estimated from three geothermometers: Bt-Cld [31], Bt-Ms [32], and Chl-Cld [33]; estimates for pressure were obtained using two modifications of the Bt-Ms-Chl geobarometer [34, 35]. For garnet-bearing metamorphic rocks of kyanite-sillimanite type, temperatures were determined by the following four calibrations for a Grt-Bt geothermometer and corresponding models of mixing: (1) Ferry and Spear [36] with mixing models by Hodges and Spear [37], (2) Perchuk and Lavrent'eva [38], (3) Kleemann and Reinhardt [39], and (4) Holdaway et al. [40]. They have analyzed eleven garnet-biotite pairs in which the coexisting minerals were not in intimate contact. Pressure estimates for these rocks were obtained using two modifications of Grt-Bt-Ms-Pl geobarometer [41, 42]. They were calculated from the Hodges—Crowley model for composition and activity [43] (for an ideal biotite solid solution and nonideal solid solutions of the other phases) and from the Hoisch model [44] (for ideal solid solutions of garnet and plagioclase and nonideal distribution of cations among octahedral positions in micas). Values of *P-T* for these rocks were calculated with the collective use of all geothermometers and geobarometers. Results of geothermobarometry are given in Table 3 and in Fig. 4. These data suggest that toward the Panimba thrust the pressure gradually grows: 3.5–4 kbar in zone I, 4.5–5 kbar in zone II, 5.5–6 kbar in zone III, and 6.2–6.7 kbar in zone IV. A slight increase in temperature (from 560 to 580 °C) near the Panimba thrust is evidence of a very small geothermal gradient during metamorphism (from 1 to 7 °C/km). Maximum temperatures (up to 600 °C) are observed for two sillimanite-bearing mineral associations (sp. 61 and 44), occurring in an intermediate zone near granites. The appearance of sillimanite seems to be connected with an insignificant increase in temperature because of the heat supplied from the intrusion [46, 47].

To estimate the reliability of geothermobarometry, these values were compared with the estimates of *P-T* conditions obtained by the "average *P-T* method" using the THERMOCALC program [48, 49] with an internally concordant thermodynamic database and Holland–Powell models for mixing [50]. The obtained results show good convergence for different zones within the accuracy of geothermobarometers: $T = \pm 50$ °C and $P = \pm 1$ kbar [51].

***P-T* paths of metamorphism.** Mineral parageneses and chemical composition of coexisting minerals show the *P-T* history of metamorphic rocks of kyanite-sillimanite type. Spear and Selverstone [52] have developed a method for calculating the *P-T* paths of evolution from zoned metamorphic minerals based on the analytical formulation of the phase equilibrium for a particular mineral assemblage permitting the use of variations of compositions of coexisting minerals for modeling changes in *P-T*. We used the PTPATH program [53] to calculate *P-T* paths for four specimens. Chemical compositions and concentration profiles of zoned garnets are reported in Table 2 and in Fig. 3.

To obtain *P-T* paths of metamorphism evolution in modeling the chemical zoning in garnets, we determined the mineral association in which garnet grew. Two specimens from an inner zone (sp. 34 and 74) are represented by the Grt+Bt+Chl+St+Ky+Ms+Pl+Qtz paranegesis. Two other specimens from the

Table 3

Estimates of *P-T* Conditions of Metamorphism of Pelites of the Korda Formation Using Different Thermobarometers

Sample no.	*T*, °C								*P*, kbar				
	[36]	[39]	[38]	[40]	[31]	[33]	[32]	[48, 49, 50]	[42]	[41]	[34]	[35]	[48, 49, 50]
Metapelites of And-Sil type (I)													
8					542	549	551				3.9 ± 0.1	3.7 ± 0.2	
10							562	553 ± 22			3.7	3.6	3.3 ± 0.7
Metapelites of Ky-Sil type (outer zone II)													
47	538	560	561	568					4.63	4.54			
51	537	561	559	573					4.83	4.66			
55	547	562	566	570				572 ± 13	5.05	4.85			4.6 ± 0.2
Metapelites of Ky-Sil type (intermediate zone III)													
63	552	567	566	582				568 ± 18	5.65	5.73			4.8 ± 1.0
61	571	574	589	598				571 ± 14	5.97	5.73			5.2 ± 0.3
44	569	577	593	601					5.87	5.77			
59	549	565	568	580				567 ± 16	5.75	5.92			5.6 ± 0.9
Metapelites of Ky-Sil type (inner zone IV)													
33	544	564	569	572					6.22	6.20			
32	550	567	570						6.30	6.29			
34	540	572	568					632 ± 40	6.38	6.42			7.6 ± 1.2
74	563	570	579	584				572 ± 16	6.68	6.70			5.9 ± 0.9

Note. Bracketed numbers of geothermobarometers are relevant references. The results obtained with the help of THERMOCALC program are given with a confidence interval ± 2σ.

intermediate zone (sp. 44 and 61) are distinguished from the two first in having additional sillimanite. The main structural feature of these specimens is the development of large pseudomorphs after andalusite, composed of the Ky+St+Ms± Sil assemblage (without garnet, chlorite, biotite, and plagioclase). The groundmass paragenesis is the Grt+Bt+Chl+Ms+Qtz+Pl assemblage. Near the periphery of pseudomorphs, these assemblages mix to form 8- and 9-mineral assemblages. These structural observations confirm that the final stages of garnet growth were related to the development of the Grt+Bt+Chl assemblage. Thus, we supposed two variants of the rock evolution: (1) Grt+Bt+Chl assemblage was ubiquitous during garnet growth and (2) Grt+And+Bt assemblage was responsible for the initial growth of garnet and was replaced by the Grt+Bt+Chl assemblage at the final stage.

It was assumed that the composition of the cores of garnet grains corresponds to the initial stage of garnet growth and gradual change in plagioclase composition was correlated with the progressive growth of garnet. The composition of rare biotite inclusions in garnet is virtually identical to the groundmass biotite composition. For this reason, as biotite inclusions cannot always be found within the cores of garnet grains, we used the core composition of groundmass biotite to determine temperature. For checking, we specially calculated *P-T* paths, using the biotite composition from the core of garnets. The calculated *P-T* paths of evolution have nearly the same form within the accuracy of the method (± 10%) [52]. This follows from analysis of mineral zoning, accounting for the form of the calculated *P-T* paths. For the majority of equilibria modeled in these calculations, temperature variations (ΔT) result from variations in X_{Fe} in garnet. A decrease in X_{Fe} usually leads to an increase in temperature (i.e., prograde dehydration), and an increase in X_{Fe} leads to the opposite effect. Since the changes in X_{Fe} in concentration profiles of garnets are small (see Table 2 and Fig. 3), the calculated variations in temperature are also negligible. If we use biotite compositions from the core of

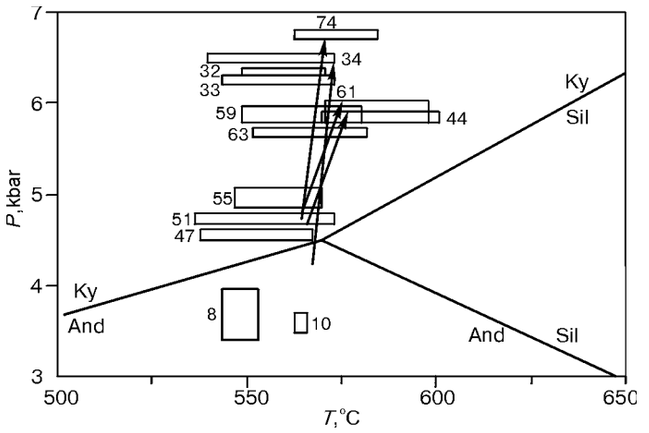

Fig. 4. *P-T* paths of metapelites of the Korda Formation near the Panimba thrust. Scatter in *P-T* estimates obtained from different geothermobarometers for each specimen is indicated by rectangles. The size of rectangles is given without consideration of the geobarometer inaccuracy. Numerals at rectangles are numbers of specimens. Directions of *P-T* paths are shown by arrows from core to rim of garnet grains and correspond to the numbers of specimens indicated near the arrow. Coordinates of triple point and lines of monovariant equilibria of aluminosilicates are given after Holland and Powell [45].

garnet, which is richer in Fe than the groundmass, this will lead to an insignificant decrease in initial temperature of garnet growth by 5–10 °C, commensurate with the accuracy of geothermometers [51]. In contrast, the considerable variations in pressure (ΔP) are the result of interaction between the content of grossular component in garnet and composition of plagioclase. Since the concentration profiles of garnets distinctly show an increased content of grossular component in a grain from core to rim, the calculated variations in pressures are quite significant.

The calculated *P-T* paths of evolution have nearly equal positive inclinations on *P-T* plots and differ only in the length of the path (see Fig. 4). They show that in all cases, toward the Panimba thrust, the pressure gradually increase (from 1 to 2 kbar) without a significant increase in temperature (up to 20± 15 °C), which can be indicative of nearly isothermal subsidence of the rocks [15]. The obtained results are well correlated with variations in mineral parageneses, structural relations between the coexisting minerals, and results of geothermobarometry.

TECTONIC MODEL AND DISCUSSION

On the basis of the above information on the character of rock metamorphism (substitution of kyanite for andalusite, increase in grossular component in garnets from core to rim, etc.) and *P-T* evolution, two stages of metamorphism can be supposed. Low-pressure andalusite schists of andalusite-sillimanite type formed at the first stage (P = 3.5–4 kbar; T = 540–560 °C). At the second stage these rocks were subjected to metamorphism with increased pressure near the thrust (P = 4.5–6.7 kbar; T = 540–600 °C). At the second stage, kyanite substituted for andalusite, and new moderate-pressure mineral parageneses of kyanite-sillimanite type formed.

To explain the pressure growth toward the thrust, several tectonic models can be proposed. 1. The metamorphic rocks participating in the structure of the region lay initially horizontally or at an angle, and they then were deformed by folding and remained either as a limb of fold or in the form of monocline. In its eastern part, they then would make up either the kernel of fold or the most subsided portion of monocline. Data of geothermometry indicate that within 5–6 km from west to east the pressure gradient is 2.2–3.2 kbar, which contradicts the lithostatic pressure under normal subsidence that could appear in these rocks at a gradient of 1 kbar/3.5 km. Moreover, as the rocks subsided, the temperature should have increased toward the thrust (from west to east), at least, by 100–120 °C, given a temperature gradient of 20 °C/km. 2. The temperature growth is caused by the tectonic stress resulting from block collision, as inferred from the intense deformation of minerals with traces of viscous flow and brittle destruction in the rocks near the thrust. However,

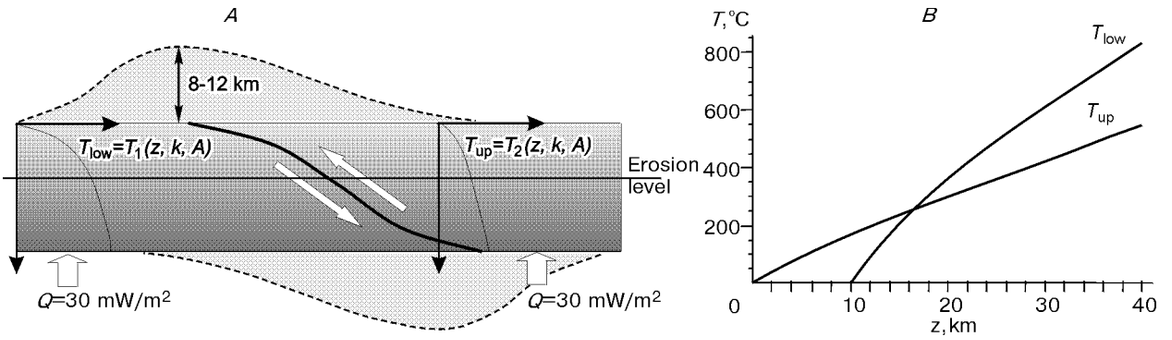

Fig. 5. Scheme of development of the Panimba thrust according to mechanism of crust thickening (*A*) and stationary distribution of temperatures in the upper and lower slabs with different thermophysical properties (*B*). Heavy line is thrust line, arrows show direction of slab shift. Mantle heat flux is supposed to be constant.

the rheology of the rocks shows that at depths of about 15–20 km, the permissible stresses are not more than 0.1–1 kbar for quartzite at geologically significant rates of deformation of 10^{-17}–10^{-14} s^{-1} [54]. These stresses are not high enough to create an extra pressure of 2.2–3.2 kbar. 3. The lithostatic pressure increased under the effect of an intrusive body (magmatic "load"). In this case, a correlation should exist between the pressure in rocks and distance to the intrusive contact (see Fig. 1, Table 3). In addition, there should have been a considerable increase in the temperature of rocks at the cost of magma crystallization (typical values for latent heat of crystallization are several orders of magnitude as high as values of heat generation by radioactive sources), which contradicts the results of geothermobarometry.

Since the above-mentioned models disagree with petrological observations, we used the hypothesis of tectonic thickening of the crust as a result of thrust [5–11, 55]. For the lithostatic pressure to be increased by 2.2–3.2 kbar, the thickness of the crust is required to be increased by 8–12 km, which implies a thrust of a rock unit subsequently removed by erosion. This thickening might be related to the process of collision of two blocks, necessarily leading to the burial of the western block of the near-fault structure under the metacarbonates of the Penchenga Formation (Fig. 5, *A*). The northeastern direction of the dip of the Panimba thrust is confirmed by the materials of the Central group of the Angara Prospecting Expedition (1986–91) on medium- and large-scale geological mapping and additional investigation into the southern part of the North-Yenisei district, and by publications of other authors on this region [17, 56], which is in agreement with our hypothesis.

We carried out the necessary calculations to justify the thrust model. It was supposed that the pressure corresponded to the lithostatic one, and temperature was found as a solution to a one-dimensional equation of heat conductivity in an infinite slab of thickness H with given parameters: surface temperature, T_S = 0, and mantle heat flow, Q = 30 mW/m^2, as boundary conditions:

$$\frac{dT}{dt} = \frac{k}{\rho C_p}\frac{\partial^2 T}{\partial z^2} + \frac{A}{\rho C_p}. \quad (1)$$

The equation of heat conductivity used the exponential distribution of radioactive sources of heat, $A = A_0 \exp(-z/D_r)$, which best of all corresponds to continental conditions [57]. To find the stationary geotherm, we integrated (1) with the zero left part, which is analytically written in the form [58]

$$T = T_S + \frac{Qz}{k} + \frac{A_0 D_r^2}{k}(1 - e^{-z/D}), \quad (2)$$

with A_0 and D_r, constants in distribution of radioactive sources; k, crust heat conductivity, and z, depth. Figure 5, *B* shows stationary geotherms in the lower and upper plate (before thrusting). This form of geotherms follows from the assumption that the coefficient of heat conductivity of metapelites (k = 1.5 W/m· K)) is lower than the heat conductivity of metacarbonates (k = 2.5 W/(m· K)) in the overthrust plate and the concentration of radioactive sources of heat in the subsurface layer of the lower plate is higher than that in the upper plate, A_0 = 3.7 against 1.7 μW/m^3. These magnitudes correspond to data on a higher heat conductivity of limestones relative to schists [59].

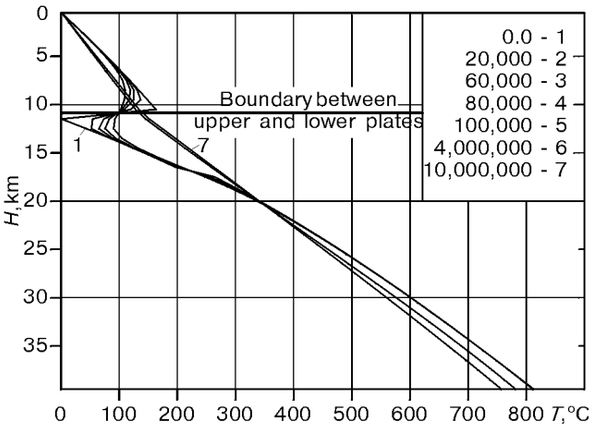

Fig. 6. Evolution of temperatures of two-layer crust after "instantaneous" thrust of a slab 8–12 km thick. Temperature isochrons 1–7 correspond to times from 0 (thrust time) to 10 Ma, shown in the inset in the top right corner of the figure. Rocks of the lower slab experience the effect of rising temperature at a depth of less than 18–20 km.

The data of geothermobarometry and calculated *P-T* paths of evolution suggest that the second stage of metamorphism was not accompanied by a considerable increase in temperature and occurred under conditions of a very low geothermal gradient (1–7 °C/km). Therefore, a hypothesized mechanism should imply the pressure growth under nearly isothermal conditions. One of the possible mechanisms discussed in literature is the thrust with the subsequent "rapid" uplift of rocks. According to this model, heat inertion prevents the temperature of submerged rocks from reaching the equilibrium temperature before they are uplifted to the surface. In agreement with the available thermophysical models [60, 61], it has been shown that the rocks of the lower plate of a near-fault structure might experienced the isothermal subduction only at a "rapid" overthrust of the upper plate (about a few meters for a million of years). Nevertheless, by tectonic interpretation of separate thrust structures in New Hampshire, Spear et al. [62] have shown that the isothermal subduction can occur in the intermediate slab sandwiched between the lower and upper plates if its confining faults move simultaneously. Temperature in this slab is kept relatively constant, since heating from above is compensated by cooling from below. However, to apply this model to our case, allochthonous rocks separated by an additional fault should lie above the Korda Formation, but this contradicts the geologic setting in the region of the Panimba thrust.

We propose another interpretation of the observed tectonometamorphic evolution of a region characterized by the regime of nearly thermal subduction. Unlike the earlier discussed models for thrust metamorphism [63], our model suggests that blocks with different thermophysical and heat-producing properties occur on both sides of the fault. Calculations show that during the "rapid" thrusting of plates with the same geotherms, the rocks of the lower plate should be warmed up for about 200 °C. However, because the rocks at different sides of the Panimba thrust are different, we may suppose different contents of radioactive sources of heat, coefficients of heat conductivity and, hence, different forms of the geotherms. Figure 6 shows the geotherm evolution in the thrust zone on the assumption of "instantaneous" overthrust of a slab 12 km thick. The one-dimensional nonstationary problem on conductive propagation of heat from the warmer upper slab to the lower one was solved by the finite-differences method [64]. The initial conditions were temperature distributions before thrusting in both slabs, corresponding to Fig. 5, *B*. After thrusting the rocks in the lower crust experienced considerable heating only within the range of depths from 12 to 18 km (see Fig. 6). Figure 6 shows that the shape of the geotherm has a slight break because of a difference in coefficients of heat conductivity of the upper and lower slabs.

To check the hypothesis of higher heat generation in metapelites relative to metacarbonates of the Penchenga Formation, the emanation of radioactive heat was calculated from data on contents of radioactive elements in rock specimens (Table 4). According to [65], the heat release from radioactive sources was averaged over five specimens, yielding $2.04 \cdot 10^{-6}$ W/m^3. This value is close to high magnitudes of heat generation for granites, $2.5 \cdot 10^{-6}$ W/m^3 [63]. For the Penchenga metacarbonates, the radioactive heat release was calculated

Table 4

Content of Radioactive Elements (U, Th, K) and Heat Generation (*A*) in Metapelites of the Korda Formation and Metacarbonates of the Penchenga Formation

Sample No.	U, ppm	Th, ppm	K, %	A, W/m^3
		Metapelites		
51	2.0	16.1	2.70	$1.93\cdot 10^{-6}$
59	2.1	14.7	2.42	$1.83\cdot 10^{-6}$
63	2.4	14.7	2.00	$1.86\cdot 10^{-6}$
34	3.1	17.0	1.65	$2.17\cdot 10^{-6}$
74	3.3	18.6	2.08	$2.38\cdot 10^{-6}$
Average A				$2.03\cdot 10^{-6}$
		Metacarbonates		
[66]	1.4	0.8	0.3	$4.39\cdot 10^{-7}$
[67]	0.4	2.1	0.6	$3.11\cdot 10^{-7}$
Average A				$3.75\cdot 10^{-7}$

Note. Average A for typical granites ($2.5\cdot 10^{-6}$). Average contents of radioactive elements for metacarbonates of the Penchenga Formation obtained from 32 and 16 gamma-spectrometric samples are given after [66] and [67], respectively.

on the basis of data from [66, 67]. The radioactive heat sources for these rocks are less powerful by an order of magnitude, about $3.75\cdot 10^{-7}$ W/m^3 (see Table 4), which supports the possibility of our mechanism. The pressure estimates for the rocks from the zone of contact with the thrust obtained from geobarometers (see Table 3), 6.2–6.7 kbar correspond to depths of 18–21 km. In this range of depths, the temperature of rocks did not virtually increase in terms of the model for tectonic thickening of the crust subduction of slabs with contrasting heat-generating properties.

CONCLUSIONS

Two stages of metamorphism have been established on the basis of detailed petrological exploration of metamorphic rocks in the trans-Angarian part of the Yenisei Ridge, in the Chirimba-Eruda interfluve. The first stage is formation of low-pressure andalusite schists of andalusite-sillimanite type (P = 3.5–4 kbar; T = 540–560 °C). The second stage is high-pressure metamorphism of these rocks near the thrust (P = 4.5–6.7 kbar; T = 540–600 °C), resulting in replacement of andalusite by kyanite and formation of new moderate-pressure metamorphic structures and mineral parageneses of kyanite-sillimanite type. The data of geothermometry and calculated P-T paths of evolution show that the second stage of metamorphism was not accompanied by a great increase in temperature and occurred under conditions of a very low geothermal gradient (1–7 °C/km), which is indicative of nearly isothermal subsidence of the rock unit. An increase in lithostatic pressure was due to a tectonic thickening of the Earth's crust in the zone of the Panimba thrust, when the Korda metapelites appeared to be buried under the Penchenga metacarbonates 8–12 km thick. Thermophysical calculations in terms of the model for tectonic thickening of the crust as a result of thrusting of slabs show that below 18 km the temperature of rocks increased insignificantly, which confirms the possibility of nearly isothermal growth of pressure during the thrust of slabs with contrasting thermophysical and heat-generating properties. This is in agreement with estimates of pressures for rocks from the zone of contact with the thrust and calculated values of heat generation for metapelites and metacarbonates.

We thank S. P. Korikovsky and V. A. Vernikovsky for constructive criticism favoring the improvement of the manuscript.

This study was supported by grant 00-05-65386 from the Russian Foundation for Basic Research.

REFERENCES

[1] D. M. Kerrick, *Miner. Soc. Amer. Reviews in Mineralogy*, vol. 22, 1990.

[2] E. N. Ushakova, *Geologiya i Geofizika*, no. 3, p. 67, 1966.
[3] I. I. Likhanov, O. P. Polyanskii, P. S. Kozlov, et al., *Dokl. RAN*, vol. 375, no. 4, p. 509, 2000
[4] L. S. Hollister, *Amer. J. Sci.*, vol. 267, p. 352, 1969.
[5] M. L. Crawford and L. E. Mark, *Can. Miner.*, vol. 20, p. 333, 1982.
[6] A. J. Baker, *J. Metamorph. Geol.*, vol. 5, p. 101, 1987.
[7] B. Beddoe-Stephens, *Scott. J. Geol.*, vol. 26, p. 3, 1990.
[8] F. S. Spear, D. D. Hickmott, and J. Selverstone, *Geol. Soc. Amer. Bull.*, vol. 102, p. 1344, 1990.
[9] G. L. Clarke, M. Guirard, R. Powell, and J. R. Burg, *J. Metamorph. Geol.*, vol. 5, p. 291, 1987.
[10] C. Ruppel and K. V. Hodge, *Tectonics*, vol. 13, p. 17, 1994.
[11] R. J. H. Loosveld and M. A. Etheridge, *J. Metamorph. Geol.*, vol. 8, p. 257, 1990.
[12] E. H. Brown and N. W. Walker, *Geol. Soc. Amer. Bull.*, vol. 105, p. 479, 1993.
[13] E. H. Brown, *J. Metamorph. Geol.*, vol. 14, p. 441, 1996.
[14] D. L. Whitney, R. B. Miller, and S. R. Paterson, *J. Metamorph. Geol.*, vol. 17, p. 75, 1999.
[15] A. B. Thompson and P. C. England, *J. Petrol.*, vol. 25, p. 929, 1984.
[16] T. Ya. Kornev, *Evolution of magmatism and ore formation* [in Russian], Moscow, 1986.
[17] P. S. Kozlov and G. G. Lepezin, *Petrology, petrochemistry, and metamorphism of rocks in the Angara region of the Yenisei Ridge*, Geologiya i Geofizika (Russian Geology and Geophysics), vol. 36, no. 5, p. 3(1), 1995.
[18] V. S. Sobolev (Ed.), *Facies of metamorphism. Vol. 1* [in Russian], Moscow, 1970.
[19] M. I. Volobuev, S. I. Zykov, and N. I. Stupnikova, in: *Geochronology of Precambrian of Siberian Platform and its folded adjacent* [in Russian], Leningrad, p. 266, 1968.
[20] E. A. Zvyagina, *Metamorphism and gold potential of Upper-Enashim ore cluster. PhD thesis* [in Russian], Irkutsk, 1989.
[21] V. S. Sobolev (Ed.), *Facies of regional high-pressure metamorphism* [in Russian], Moscow, 1974.
[22] R. Kretz, *Amer. Miner.*, vol. 68, p. 277, 1983.
[23] D. M. Carmichael, *Contr. Miner. Petrol.*, vol. 20, p. 244, 1969.
[24] B. W. D. Yardley, *An Introduction to Metamorphic Petrology*, Harlow, 1989.
[25] J. J. Ague, *Geology*, vol. 19, p. 855, 1991.
[26] D. M. Shaw, *Geol. Soc. Amer. Bull.*, vol. 67, p. 913, 1956.
[27] G. H. Symmes and J. M. Ferry, *J. Metamorph. Geol.*, vol. 10, p. 221, 1992.
[28] J. B. Thompson, Jr., *Amer. Miner.*, vol. 42, p. 842, 1957.
[29] M. J. Holdaway, B. L. Dutrow, and R. W. Hinton, *Amer. Miner.*, vol. 73, p. 20, 1988.
[30] F. S. Spear, *Geol. Soc., London*, Special Publication 43, p. 63, 1989.
[31] L. L. Perchuk, in: *Progress in Metamorphic and Magmatic Petrology*, Cambridge, p. 93, 1991.
[32] T. D. Hoisch, *Amer. Miner.*, vol. 74, p. 565, 1989.
[33] O. Vidal, B. Goffe, R. Bousquet, and T. Parra, *J. Metamorph. Geol.*, vol. 17, p. 25, 1999.
[34] R. Powell and J. A. Evans, *J. Metamorph. Geol.*, vol. 1, p. 331, 1983.
[35] K. Bucher-Nurminen, *Contr. Miner. Petrol.*, vol. 96, p. 519, 1987.
[36] J. M. Ferry and F. S. Spear, *Contr. Miner. Petrol.*, vol. 66, p. 113, 1978.
[37] K. V. Hodges and F. S. Spear, *Amer. Miner.*, vol. 67, p. 1118, 1982.
[38] L. L. Perchuk and I. V. Lavrent'eva, in: *Kinetics and Equilibrium in Mineral Reactions*, Berlin—Heidelberg—New York, p. 199, 1983.
[39] U. Kleemann and J. Reinhardt, *European J. Miner.*, vol. 6, p. 925, 1994.
[40] M. J. Holdaway, B. Mukhopadhyay, M. D. Dyar, et al., *Amer. Miner.*, vol. 82, p. 582, 1997.
[41] T. D. Hoisch, *Contr. Miner. Petrol.*, vol. 104, p. 225, 1990.
[42] E. D. Ghent and M. Z. Stout, *Contr. Miner. Petrol.*, vol. 76, p. 92, 1981.
[43] K. V. Hodges and P. D. Crowley, *Amer. Miner.*, vol. 70, p. 702, 1985.
[44] T. D. Hoisch, *Contr. Miner. Petrol.*, vol. 108, p. 43, 1991.
[45] T. J. B. Holland and R. Powell, *J. Metamorph. Geol.*, vol. 3, p. 343, 1985.
[46] I. I. Likhanov, V. S. Sheplev, V. V. Reverdatto, and P. S. Kozlov, *Dokl. RAN*, vol. 362, p. 673, 1998.
[47] I. I. Likhanov, V. S. Sheplev, V. V. Reverdatto, et al., *The isochemical nature of the contact metamorphism of high-alumina metapelites in the Ayakhta granitoid massif, Yenisei Range*, Geologiya i Geofizika (Russian Geology and Geophysics), vol. 40, no. 1, p. 90(91), 1999.
[48] R. Powell and T. J. B. Holland, *J. Metamorph. Geol.*, vol. 6, p. 173, 1988.
[49] R. Powell and T. J. B. Holland, *Amer. Miner.*, vol. 79, p. 120, 1994.
[50] T. J. B. Holland and R. Powell, *J. Metamorph. Geol.*, vol. 6, p. 89, 1990.

[51] E. J. Essene, *Geol. Soc., London*, Special Publication 43, p. 1, 1989.
[52] F. S. Spear and J. Selverstone, *Contr. Miner. Petrol.*, vol. 83, p. 348, 1983.
[53] F. S. Spear, *Computers and Geosciences*, vol. 12, p. 247, 1986.
[54] J. Strehlau and R. Meissner, in: *Compositions, Structure and Dynamics of the Lithosphere-Asthenosphere System, Geodyn. Ser.*, AGU, Washington, D.C., vol. 16, p. 69, 1987.
[55] P. C. England and A. B. Thompson, *J. Petrol.*, vol. 25, p. 894, 1984.
[56] D. L. Turcotte and G. Shubert, *Geodynamics. Applications of continuum physics to geological problems*, New York, 1982.
[57] C. A. Smit, D. D. Van Reenen, T. V. Gerya, et al., *Miner. Petrol.*, vol. 69, p. 35, 2000.
[58] F. S. Spear, *Metamorphic phase equilibria and pressure—temperature—time paths. Miner. Soc. Amer.*, Washington, D.C., 1993.
[59] S. Clark (Ed.), *Handbook of physical constants* [Russian translation], Moscow, 1969.
[60] Y. Shi and C. Wang, *Geology*, vol. 15, p. 1048, 1987.
[61] P. Karabinos and R. Ketchman, *J. Metamorph. Geol.*, vol. 6, p. 559, 1988.
[62] F. S. Spear, M. J. Kohn, and T. M. Harrison, *Geol. Soc. Amer. (Abstracts with Programs)*, vol. 21, p. 67, 1989.
[63] S. M. Peacock, *Geol. Soc. Amer. Bull.*, vol. 101, p. 476, 1989.
[64] D. O. Hayba and S. E. Ingebritsen, *J. Geophys. Res.*, vol. 102, p. 12235, 1997.
[65] E. A. Lyubimova, *Thermal parameters of the Earth and the Moon* [in Russian], Moscow, 1968.
[66] V. A. Zlobin, A. A. Kulikov, and V. A. Bobrov, in: *Radioactive elements in rocks* [in Russian], Novosibirsk, p. 198, 1975.
[67] A. D. Nozhkin, F. P. Krendelev, and A. G. Mironov, *ibid.*, p. 183.

Recommended by V. S. Shatsky

Received 15 September 2000
Accepted 17 January 2001